Combined half-integer Bessel-like beams: A set of solutions of the wave equation

Davud Hebri[1] and Saifollah Rasouli[1,2,*]

[1]*Department of Physics, Institute for Advanced Studies in Basic Sciences (IASBS), Zanjan 45137-66731, Iran*

[2]*Optics Research Center, Institute for Advanced Studies in Basic Sciences (IASBS), Zanjan 45137-66731, Iran*

(Received 15 May 2018; published 12 October 2018)

We report a family of solutions of the homogeneous free-space scalar wave equation. These solutions are determined by linear combinations of the half-integer order Bessel functions. We call these beams "combined half-integer Bessel-like beams." It is shown that, by selecting suitable combinations of the half-integer order Bessel functions, a wide set of beams can be produced in which they may carry the orbital angular momentum (OAM) or not. We show that this family of beams satisfies a "radial structured" boundary condition at $z = 0$ plane, therefore they can be produced by the diffraction of a plane wave from suitable "radial structures." Some specific examples of the half-integer Bessel-like beams are introduced. Especially, a set of spatially asymmetric beams, having half-integer OAM, is introduced that can be used to make the concentration of the absorbing and dielectric micro- or nanoparticles in a microsolution inhomogeneous. Also, by manipulating the Fourier series of the radial structures, three subfamily of beams can be produced including the radial carpet, petallike, and ringlike vortex beams. The intensity profile of the petallike beams forms two dimensional optical latices with polar symmetry at the transverse plane. The ringlike vortex beams carry OAM. Here, by solving the wave equation we present the full image of the radial carpet beams. All the presented beams have nondiffracting, accelerating, and self-healing features. The combined half-integer Bessel-like beams can be considered in other areas of wave phenomena, ranging from sound and elastic waves to many other kinds of classical waves. Therefore, this work has profound implications in many linear wave systems in nature.

DOI: 10.1103/PhysRevA.98.043826

I. INTRODUCTION

The wave equation is one of the greatest findings in science and mathematics. It is a second-order linear partial differential equation that explains the wave phenomena in classical physics. The wave equation is used for describing wave phenomena in acoustics, electromagnetism, and fluid dynamics. The electromagnetic wave equation delivered by James Clerk Maxwell by creatively combining the Maxwell's equations describes the propagation of electromagnetic waves through a vacuum (with a speed equal to the speed of light) and a medium.

In recent decades, a number of solutions of the free-space homogeneous wave equation have been discovered. Paraxial approximation plays an important role in studying the optical beam propagation [1]. An optical wave whose wavefront normals make small angles with the main propagation axis z is known as a paraxial wave and satisfies the paraxial Helmholtz equation. One of the famous solutions of the paraxial Helmholtz equation is the Gaussian beam that provides all aspects of an optical beam. Various closed-form solutions of the paraxial wave equation have been obtained, including the standard and elegant Hermite-Gaussian beams [2], Laguerre-Gaussian beams [3,4], Ince-Gaussian beams [5,6], Hermite-Laguerre-Gaussian beams [7,8], Helmholtz-Gauss and Laplace-Gauss beams [9], hypergeometric Gaussian beams [10], and the Cartesian and circular beams [11,12].

Among various solutions found for the wave equation, the diffraction-free beams are attracting major attention. These beams are presenting applications in many areas such as laser manipulation and patterning, plasma channels, and light-sheet microscopy. A well-known diffraction-free wave is the Bessel beam [13,14]. There are a number of nondiffracting beams such as parabolic waves [15], the Mathieu beams [16], Airy beam [17,18], Airy-Gaussian beams [19], Bessel X waves, and Bessel-like beams [20–22].

In a recent paper, in the context of diffraction from radial gratings, a class of nondiffracting, accelerating, and self-healing beams, the so called "radial carpet beams" were introduced in Ref. [23]. The theory of that work is based on solving of the Fresnel-Kirchhoff integral. In that work, the generation of unprecedented 2D optical lattices with polar symmetry was also reported. It was shown that these optical carpet patterns and 2D optical lattices are shape-invariant and self-healing for more than several hundreds of meters.

It is worth mentioning that in a number of close works some aspects of the diffraction of plane and vortex beams from radial amplitude gratings have recently been reported [24,25].

In this work we obtain a family of solutions of the paraxial wave equation and show that the "radial carpet beams" are a subset of the solutions obtained.

This family of solutions of the paraxial wave equation consisting of different subfamily of beams with interesting features. In this work we investigate a set of spatially asymmetric beams carrying half-integer OAM and a set of ringlike vortex beams having OAM. Suitable experimental approaches are proposed to generate such beams.

*rasouli@iasbs.ac.ir

II. PARAXIAL HELMHOLTZ EQUATION

Considering $U(x, y, z)$ as the complex amplitude of a monochromatic light beam, we know that it satisfies the following differential equation, known as the Helmholtz equation:

$$\nabla^2 U + k^2 U = 0, \tag{1}$$

where $k = \frac{2\pi}{\lambda}$ is the wave number. The complex amplitude of a paraxial wave traveling along the z direction can be written as follows:

$$U(x, y, z) = A(x, y, z)\exp(ikz), \tag{2}$$

where $A(x, y, z)$ is a slowly varying envelop function. By substituting Eq. (2) into Eq. (1) and using paraxial approximation, the following paraxial Helmholtz equation is obtained [26]:

$$\nabla_T^2 A + 2ik\frac{\partial A}{\partial z} = 0, \tag{3}$$

where $\nabla_T^2 = \frac{\partial^2}{\partial x^2} + \frac{\partial^2}{\partial y^2}$ is the transverse Laplacian operator. The paraxial approximation to the scalar Helmholtz equation is equivalent to the Schrodinger equation of a free particle. There are various families of solutions for this equation. The Hermit-Gaussian beams form a well-known complete set of its solutions. By using the ∇_T^2 form in the cylindrical coordinates we get

$$\frac{1}{r}\frac{\partial}{\partial r}\left(r\frac{\partial A}{\partial r}\right) + \frac{1}{r^2}\frac{\partial^2 A}{\partial \theta^2} + 2ik\frac{\partial A}{\partial z} = 0, \tag{4}$$

which is known as the paraxial Helmholtz equation in the cylindrical coordinates. A conventional complete set of solutions for this equation, known as the Laguerre-Gaussian beams, is obtained using the separation-of-variables technique in r and θ, rather than in x and y.

III. COMBINED HALF-INTEGER BESSEL-LIKE BEAMS: A SET OF SOLUTIONS FOR THE PARAXIAL HELMHOLTZ EQUATION IN THE CYLINDRICAL COORDINATES

Here an alternate complete set of solutions for Eq. (4) is presented. To separate the azimuthal dependency, the following form of solution is considered:

$$A(r, \theta, z) = g(\rho)\exp(in\theta), \tag{5}$$

where $\rho = \rho(r, z) = \frac{kr^2}{4z}$ is a dimensionless parameter, and n is an integer. By substituting Eq. (5) in Eq. (4) we can get

$$r\frac{\partial}{\partial r}\left(r\frac{\partial g}{\partial r}\right) + 2ikr^2\frac{\partial g}{\partial z} - n^2 g = 0. \tag{6}$$

It is clear that this is a partial differential equation (PDE) in terms of the coordinates (r, z). Since we have $\frac{\partial \rho}{\partial r} = \frac{k}{2z}r = \frac{2\rho}{r}$ or $r\frac{\partial \rho}{\partial r} = 2\rho$ and $\frac{\partial \rho}{\partial z} = -\frac{kr^2}{4z^2} = -\frac{\rho}{z}$, and using the chain rule we can easily obtain the following derivative identities:

$$r\frac{\partial g}{\partial r} = r\frac{dg}{d\rho}\times\frac{\partial \rho}{\partial r} = 2\rho\frac{dg}{d\rho}, \tag{7}$$

$$r\frac{\partial}{\partial r}\left(r\frac{\partial g}{\partial r}\right) = r\frac{d}{d\rho}\left(2\rho\frac{dg}{d\rho}\right)\times\frac{\partial \rho}{\partial r} = 4\rho\frac{d}{d\rho}\left(\rho\frac{dg}{d\rho}\right), \tag{8}$$

$$\frac{\partial g}{\partial z} = \frac{dg}{d\rho}\times\frac{\partial \rho}{\partial z} = -\frac{\rho}{z}\frac{dg}{d\rho}, \tag{9}$$

and

$$2ikr^2\frac{\partial g}{\partial z} = -\frac{2ikr^2}{z}\rho\frac{dg}{d\rho} = -8i\rho^2\frac{dg}{d\rho}, \tag{10}$$

where $\rho = \frac{kr^2}{4z}$ is used. Using Eqs. (8) and (10) in Eq. (6) we have

$$\frac{1}{\rho}\frac{d}{d\rho}\left(\rho\frac{dg}{d\rho}\right) - 2i\frac{dg}{d\rho} - \frac{(n/2)^2}{\rho^2}g = 0, \tag{11}$$

which is an ordinary differential equation (ODE) in terms of ρ. In the following this ODE is solved.

Let us now write $g(\rho)$ in terms of a new function $f(\rho)$:

$$g(\rho) = \sqrt{\rho}\exp(i\rho)f(\rho). \tag{12}$$

Substituting Eq. (12) in Eq. (11) we get

$$f'' + \frac{2}{\rho}f' + f + \frac{i}{\rho}f + \frac{1-n^2}{4\rho^2}f = 0, \tag{13}$$

where $f' = \frac{df}{d\rho}$ and $f'' = \frac{d^2 f}{d\rho^2}$ are the first and second derivatives of $f(\rho)$, respectively. As one of the coefficients in Eq. (13) is complex, a complex solution can be proposed with the following form:

$$f(\rho) = f_r(\rho) + i\,f_i(\rho), \tag{14}$$

where $f_r(\rho)$ and $f_i(\rho)$ are the real and imaginary parts of $f(\rho)$. By substituting this form of solution in Eq. (13), the following two coupled ODEs are obtained:

$$f_r{}'' + \frac{1}{\rho}f_r{}' + f_r + \frac{1}{\rho}(f_r{}' - f_i) + \frac{1-n^2}{4\rho^2}f_r = 0 \tag{15}$$

and

$$f_i{}'' + \frac{1}{\rho}f_i{}' + f_i + \frac{1}{\rho}(f_i{}' + f_r) + \frac{1-n^2}{4\rho^2}f_i = 0. \tag{16}$$

The first three terms of both of these ODEs are the same as the first three terms of Bessel's differential equation given by

$$J_\nu{}'' + \frac{1}{\rho}J_\nu{}' + J_\nu = \frac{\nu^2}{\rho^2}J_\nu, \tag{17}$$

where $J_\nu = J_\nu(\rho)$ indicates the Bessel function of the first kind. Let us remember two basic Bessel-function recurrence relations [27],

$$J'_\nu - J_{\nu-1} = -\frac{\nu}{\rho}J_\nu \tag{18}$$

and

$$J'_{\nu-1} + J_\nu = \frac{\nu-1}{\rho}J_{\nu-1}. \tag{19}$$

Now considering that $f_r(\rho) = J_\nu(\rho)$ and $f_i(\rho) = J_{\nu-1}(\rho)$, and using Eqs. (17)–(19) in Eqs. (15) and (16), the following identities are obtained:

$$\nu^2 - \nu = \frac{n^2-1}{4} \tag{20}$$

and

$$(\nu-1)^2 + (\nu-1) = \frac{n^2-1}{4}. \tag{21}$$

Both of the equations lead to the same quadratic equation in terms of ν,

$$\nu(\nu-1) = \left(\frac{n}{2}+\frac{1}{2}\right)\left(\frac{n}{2}-\frac{1}{2}\right). \tag{22}$$

This equation has two roots, $\nu_1 = \frac{n+1}{2}$ and $\nu_2 = \frac{-n+1}{2}$. Accordingly, the following two solutions for $f(\rho)$ are obtained:

$$f_1(\rho) = J_{\frac{n+1}{2}}(\rho) + iJ_{\frac{n-1}{2}}(\rho), \tag{23}$$

$$f_2(\rho) = J_{\frac{-n+1}{2}}(\rho) + iJ_{\frac{-n-1}{2}}(\rho). \tag{24}$$

Since Eq. (13) is a linear homogeneous ODE, any linear combination of its solutions, say $f(\rho) = af_1(\rho) + bf_2(\rho)$, is also a solution. Therefore, the general solution is

$$f(\rho) = a_n\left[J_{\frac{n+1}{2}}(\rho) + iJ_{\frac{n-1}{2}}(\rho)\right] + b_n\left[J_{\frac{-n+1}{2}}(\rho) + iJ_{\frac{-n-1}{2}}(\rho)\right], \tag{25}$$

where a_n and b_n are arbitrary constants. Now, according to Eqs. (5) and (12), one can write

$$A_n(\rho,\theta) = \sqrt{\rho}e^{i\rho}e^{in\theta}\left\{a_n\left[J_{\frac{n+1}{2}}(\rho) + iJ_{\frac{n-1}{2}}(\rho)\right] + b_n\left[J_{\frac{-n+1}{2}}(\rho) + iJ_{\frac{-n-1}{2}}(\rho)\right]\right\}. \tag{26}$$

Since the original PDE, introduced as Eq. (3), is linear and homogeneous, we can develop the most general solution of Eq. (3) by taking a linear combination of the solutions

$$A(\rho,\theta) = \sqrt{\rho}e^{i\rho}\left\{\sum_{n=-\infty}^{\infty} a_n e^{in\theta}\left[J_{\frac{n+1}{2}}(\rho) + iJ_{\frac{n-1}{2}}(\rho)\right] + b_n e^{in\theta}\left[J_{\frac{-n+1}{2}}(\rho) + iJ_{\frac{-n-1}{2}}(\rho)\right]\right\}. \tag{27}$$

Rearranging, this result can be rewritten as follows:

$$A(\rho,\theta) = \sqrt{\rho}e^{i\rho}\sum_{n=-\infty}^{\infty}(a_n e^{in\theta} + b_n e^{-in\theta}) \times \left[J_{\frac{n+1}{2}}(\rho) + iJ_{\frac{n-1}{2}}(\rho)\right], \tag{28}$$

where b_n in Eq. (28) corresponds to b_{-n} in Eq. (27).

Here we show that summation in Eq. (28) may be over the range of n from 0 to ∞, without loss of generality. For this purpose we can rewrite Eq. (28) as

$$A(\rho,\theta) = \sqrt{\rho}e^{i\rho}\left\{\sum_{n=0}^{\infty}(a_n e^{in\theta} + b_n e^{-in\theta})\left[J_{\frac{n+1}{2}}(\rho) + iJ_{\frac{n-1}{2}}(\rho)\right] + \sum_{n=1}^{\infty}(a_{-n}e^{-in\theta} + b_{-n}e^{in\theta})\left[J_{\frac{-n+1}{2}}(\rho) + iJ_{\frac{-n-1}{2}}(\rho)\right]\right\}, \tag{29}$$

where in the last summation we replaced $-n$ with n.

For the odd values of n, $\frac{n\pm1}{2}$ is an integer number, and it is easy to show that $J_{\frac{-n\mp1}{2}} = J_{-\frac{n\pm1}{2}} = (-1)^{\frac{n\pm1}{2}}J_{\frac{n\pm1}{2}}$ by considering the well-known identity $J_{-m} = (-1)^m J_m$ for integer values of m. Therefore, for the odd values of n, the second summation can be derived with the first summation, and it can be ignored without loss of generality. Also, for the even values of n, we show that we need to ignore the last summation to serve the physical validity of the solutions. In this case $\frac{-n\pm1}{2}$ is a negative half-integer number, and it can be shown that for a Bessel function with a negative half-integer order, the value of $\sqrt{\rho}J_{\frac{-n\pm1}{2}}(\rho)$ diverges at the origin. Hence, the second summation should be ignored to grantee the physical validity of the results.

Finally, using Eq. (2), the following result is obtained:

$$U(r,\theta,z) = e^{ikz}\sqrt{\rho}e^{i\rho}\sum_{n=0}^{\infty}(a_n e^{in\theta} + b_n e^{-in\theta}) \times \left[J_{\frac{n+1}{2}}(\rho) + iJ_{\frac{n-1}{2}}(\rho)\right]. \tag{30}$$

This equation represents a family of solutions of the paraxial Helmholtz equation, Eq. (3). Based on the form of these solutions, we call the resulting beams "combined half-integer Bessel-like beams." Equation (30) shows that the spatial structure of half-integer Bessel-like beams is preserved under propagation.

Making use of the following reference relationships [28]:

$$J_{\frac{1}{2}}(x) = \sqrt{\frac{2}{\pi x}}\sin(x), \qquad J_{-\frac{1}{2}}(x) = \sqrt{\frac{2}{\pi x}}\cos(x), \tag{31}$$

one can write

$$J_{\frac{1}{2}}(\rho) + iJ_{-\frac{1}{2}}(\rho) = i\sqrt{\frac{2}{\pi\rho}}\exp(-i\rho). \tag{32}$$

Using this identity, Eq. (30) can be rewritten as follows:

$$U(r,\theta,z) = e^{ikz}\left\{t_0 + \sqrt{\rho}e^{i\rho}\sum_{n=1}^{+\infty}(a_n e^{in\theta} + b_n e^{-in\theta}) \times \left[J_{\frac{n+1}{2}}(\rho) + iJ_{\frac{n-1}{2}}(\rho)\right]\right\}, \tag{33}$$

where $t_0 = \sqrt{\frac{2}{\pi}}(a_0 + b_0)i$.

IV. BOUNDARY CONDITION AT $z = 0$ PLANE

Let us now calculate $U(x, y, z = 0)$. As $\rho \propto \frac{1}{z}$, for $z \to 0$ the value of ρ goes to infinity. For large values of ρ the Bessel function can be written as

$$J_\nu(\rho) \to \sqrt{\frac{2}{\pi\rho}}\cos\left(\rho - \frac{\nu\pi}{2} - \frac{\pi}{4}\right), \tag{34}$$

and therefore

$$\left[J_{\frac{n+1}{2}}(\rho) + iJ_{\frac{n-1}{2}}(\rho)\right] \to i^{\frac{n}{2}+1}\sqrt{\frac{2}{\pi\rho}}\exp(-i\rho). \tag{35}$$

Now using this result we obtain

$$U(r,\theta,z=0) = t(\theta) = t_0 + \sum_{n=1}^{+\infty}(t_n\, e^{in\theta} + t_{-n}e^{-in\theta}), \tag{36}$$

where $t_n = i^{\frac{n}{2}+1}\sqrt{\frac{2}{\pi}}a_n$ and $t_{-n} = i^{\frac{n}{2}+1}\sqrt{\frac{2}{\pi}}b_n$. The main feature of this result is that it has no radial dependency and can be considered as the transmitted amplitude of a plane wave immediately after a radial structure. A structure is defined as a "radial structure" when there is no radial dependency in its transmission function (see Refs. [23,24]). Now we assume that the complex amplitude of the light beam at $z = 0$ plane has a radial structure, say $U(x, y, z = 0) = t(\theta)$. Using the

Fresnel-Kirchhoff integral, the propagation of such light beam can be written in the following form [24]:

$$U(r,\theta,z) = e^{ikz}\Bigg\{t_0 + \sqrt{\rho}e^{i\rho}\sum_{n=1}^{+\infty}\sqrt{\frac{\pi}{2}}(-i)^{\frac{n}{2}+1} \times (t_n e^{in\theta} + t_{-n}e^{-in\theta})\Big[J_{\frac{n+1}{2}}(\rho) + iJ_{\frac{n-1}{2}}(\rho)\Big]\Bigg\}, \tag{37}$$

where k and ρ are the same parameters that were used above.

Now, let us compare this complex amplitude with the one obtained directly from the wave equation, Eq. (33). If we set $t_n = i^{\frac{n}{2}+1}\sqrt{\frac{2}{\pi}}a_n$ and $t_{-n} = i^{\frac{n}{2}+1}\sqrt{\frac{2}{\pi}}b_n$ in Eq. (37), then the result will be exactly the same as Eq. (33). This means that the complex amplitudes obtained from both the wave equation and Fresnel integral are the same at any propagation distance. It is worth mentioning that although the paraxial approximation may be violated at the vicinity of $z = 0$, this equality guarantees that the form of light field at $z = 0$ in Eq. (36) is correctly obtained from Eq. (33). Below, the validity of the paraxial approximation at the vicinity of $z = 0$ will be investigated.

V. SOME GENERAL FEATURES OF THE COMBINED HALF-INTEGER BESSEL-LIKE BEAMS

As it is seen from Eqs. (33) and (37) the complex amplitude of the half-integer Bessel-like beams at a given z is a function of $\rho = \frac{kr^2}{4z}$. Therefore, the whole pattern of a given beam expands with a factor $\sqrt{z}$ during propagation, and the rate of the pattern size increment is $\frac{1}{2\sqrt{z}}$, which is a descending function of z. Therefore, although the size of the half-integer Bessel-like beams increases by a factor $\sqrt{z}$, the rate of the pattern size increment or equally the cone angle of the beam, decreases with propagation. This behavior shows the nondiffractive feature of the half-integer Bessel-like beams. Moreover, the trajectory of a given point under propagation may be obtained by following it on the intensity pattern of a beam for a given value of ρ. For a point on the intensity pattern with a radius r_0 at a given propagation distance of z_0, its radius r at an arbitrary propagation distance of z can be calculated and the trajectory of the point is given by

$$r(z) = \frac{r_0}{\sqrt{z_0}}\sqrt{z}. \tag{38}$$

This equation determines the position of a given point on the beam under propagation, and can be considered as the ray equation. This means that the propagation path of a given point on the intensity pattern is a curve path being concave toward the optical axis. As the beams expand with unequal rate with distance z, they are accelerating.

VI. SOME SIMPLE OBJECTIVE EXAMPLES

It is important to provide some objective examples of the half-integer Bessel-like beams. As the simplest case, we set all coefficients in Eq. (36) equal to zero except for $t_m = 1$. Then

$$t(\theta) = \exp(im\theta), \tag{39}$$

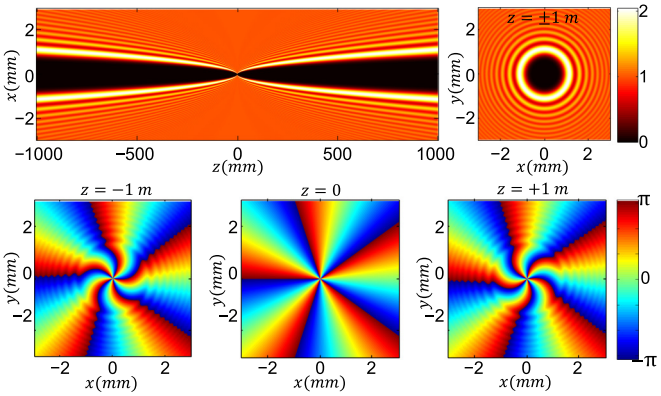

FIG. 1. First row: Intensity patterns at the longitudinal (left) and transverse (right) planes for a half-integer Bessel-like beam with $t_{m=5} = 1$ and with other coefficients equal to zero (a beam produced by an SPP). Second row: Corresponding phase profiles at the transverse planes at locations $z = -1$ m, $z = 0$, and $z = +1$ m.

which describes a spiral phase plate (SPP) with mth order singularity. Substituting Eq. (39) in Eq. (33) or Eq. (37), corresponding light beam is

$$U = u_m e^{i(kz+\rho+m\theta)}\sqrt{\rho}\Big[J_{\frac{m+1}{2}}(\rho) + iJ_{\frac{m-1}{2}}(\rho)\Big], \tag{40}$$

where $u_m = \sqrt{\frac{\pi}{2}}(-i)^{\frac{m}{2}+1}$. Since Eq. (40) is a result of the wave equation, it can be used to investigate the treatment of the beam for both positive and negative values of z. In Fig. 1 the intensity and phase patterns of a half-integer Bessel-like beam with $m = 5$ are illustrated. This light field indicates a vortex beam which carries OAM with a topological charge of order m. As is apparent from Fig. 1, the intensity pattern is symmetric with respect to the $z = 0$ plane, but the phase distributions are slightly different over two transverse planes of $z = \pm 1$ m. Also, it is seen that at large values of r, the phase and intensity profiles reach their values at $z = 0$ plane, which means that for $r \gg 0$ the light beam structure remains unchanged under propagation. Diffraction of a plane or a Gaussian beam from an SPP using the Fresnel integral is presented in Ref. [29]. Using two different approaches, the first based on mathematical approximation [29] and the second on physical reasoning [24], the vortex core size or radius of the first intensity maximum for this beam can be estimated to be

$$r_m \approx \sqrt{\frac{(m+1)\lambda z}{2}} \tag{41}$$

and

$$r_m \approx \sqrt{\frac{m\lambda z}{\pi}}, \tag{42}$$

respectively. Both the above estimations have the same dependency on z which consists with Eq. (38).

Now we check the validity of the paraxial approximation when $z \to 0$. We know that a wave is called paraxial if its wavefront normals (rays) make small angles with the z axis [26]. Using Eq. (42) as a ray path equation [or equivalently Eq. (41)] we can calculate the angle this ray makes with the z axis, say, $\frac{\partial r_m}{\partial z} \approx \sqrt{\frac{m\lambda}{4\pi z}}$. We see that for $z \to 0$ we have $\frac{\partial r_m}{\partial z} \to \infty$, this means that there is a collapse for the rays at $z = 0$ (see

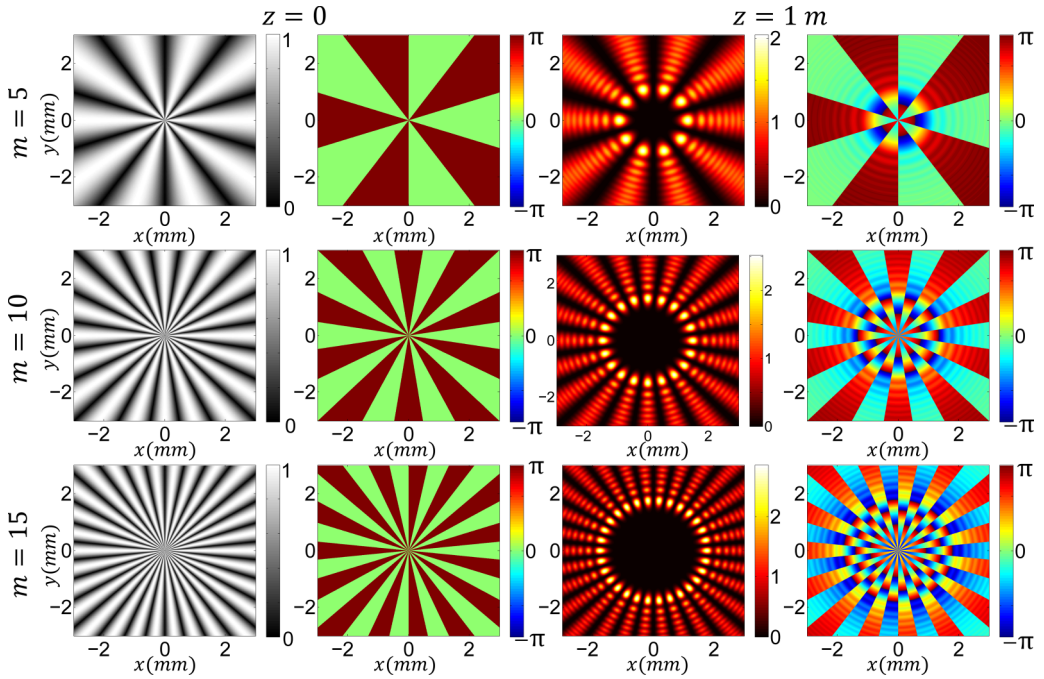

FIG. 2. First and second columns: Absolute value and phase patterns of $t(\theta) = \cos(m\theta)$ for different values of m. Third and forth columns: Corresponding beams' intensity and phase patterns at $z = 1$ m.

the rays paths in Fig. 1). Since in the paraxial approximation $\frac{\partial r_m}{\partial z} \ll 1$ then $\sqrt{\frac{m\lambda}{4\pi z}} \ll 1$ or $z \gg m\lambda$. Therefore, at $|z| \gg m\lambda$, Eq. (40) describes the behavior of light field.

As another simple example of Eq. (36) we consider the following combination:

$$t(\theta) = \cos(m\theta) = \tfrac{1}{2}(e^{im\theta} + e^{-im\theta}). \tag{43}$$

This is a real transmission function and can be considered to be a linear combination of two SPPs having opposite orders. As the sign of the transmission function alternates periodically, it does not indicate a pure amplitude structure. To determine its phase and absolute value, we rewrite it in the following form:

$$t(\theta) = |\cos(m\theta)|e^{i\delta(\theta)}, \tag{44}$$

where the phase $\delta(\theta)$ is a binary periodic function alternating between 0 and π with a period of $\frac{2\pi}{m}$, and $|\cos(m\theta)|$ being the absolute value of the transmittance having a period of $\frac{\pi}{m}$. In Fig. 2, the first and second columns show the absolute value and phase of this transmittance, respectively, for the different values of m at the different rows. Unlike an SPP, this transmittance does not impose OAM on an incident plane wave. Comparing Eqs. (43) and (36), we see that $t_m = t_{-m} = \frac{1}{2}$ and all other coefficients are zero. Therefore, the corresponding light beam is given by

$$U(r, \theta, z) = u_m e^{i(kz+\rho)}\sqrt{\rho}\left[J_{\frac{m+1}{2}}(\rho) + iJ_{\frac{m-1}{2}}(\rho)\right]\cos(m\theta), \tag{45}$$

where $u_m = \sqrt{\frac{\pi}{2}}(-i)^{\frac{m}{2}+1}$. In Fig. 2, the third and forth columns show the intensity and phase patterns of the beam at $z = 1$ m, respectively. The patterns in each row correspond to a given value of m. As is apparent these beams have petallike intensity profiles. In practice, using a pure radial amplitude grating and an SLM such beams can be easily produced. Further details are beyond the scope of the current work.

Spatially asymmetric beams

As another combination of different terms of Eq. (36), we consider the superposition of two SPPs having different orders:

$$t(\theta) = \tfrac{1}{2}(e^{im\theta} + e^{in\theta}). \tag{46}$$

Using the Euler's formula and sum-to-product trigonometric identities this reduces to

$$t(\theta) = \cos\left(\frac{m-n}{2}\theta\right)\exp\left(i\frac{m+n}{2}\theta\right). \tag{47}$$

Here again to determine the phase and absolute value of $t(\theta)$, we rewrite it in the following form:

$$t(\theta) = \left|\cos\left(\frac{m-n}{2}\theta\right)\right|\exp\left[i\phi(\theta)\right], \tag{48}$$

in which $\phi(\theta)$ is the phase of the transmittance calculated using

$$\phi(\theta) = \delta(\theta) + \frac{m+n}{2}\theta, \tag{49}$$

where $\delta(\theta)$ is a binary periodic function alternating between 0 and π with a period of $\frac{4\pi}{m-n}$. The light beam topological charge can be calculated using $\frac{1}{2\pi}\oint_C \nabla\phi.dr$, with loop C enclosing the singularity (here the origin). As the term $\delta(\theta)$ does not lead to a pure change in the phase over a cycle, this transmittance imposes an OAM on an incident plane wave with a topological charge of order $\frac{m+n}{2}$. When both m and n are even or odd, the order of the topological charge of the beam is integer. When

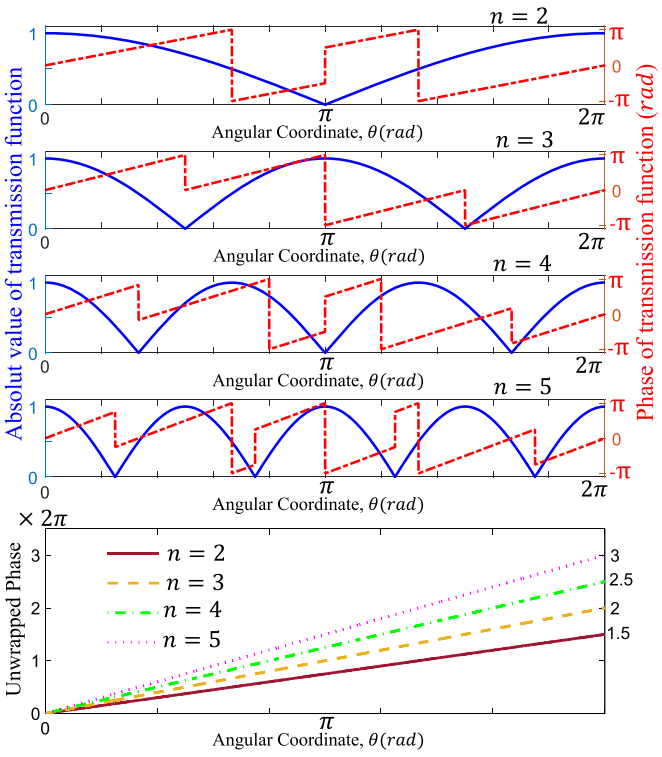

FIG. 3. First to forth rows: Absolute value (blue solid line) and phase (red dash line) profiles of $t(\theta) = \frac{1}{2}(e^{im\theta} + e^{in\theta})$ for $n = 2, 3, 4, 5$ and $m = 1$, respectively. Fifth row: The corresponding unwrapped phase profiles.

one of the m or n is even and other one is odd, the beam has a half-integer topological charge. Using the fact that OAM is preserved under free space propagation the above calculated result can be used for all propagation distances [30].

Figure 3 shows the absolute value and phase profiles of $t(\theta)$ for $m = 1$ and $n = 2, 3, 4, 5$. The last row shows corresponding unwrapped phase profiles. Looking at these unwrapped phase profiles we see that, in each case, the pure phase change over a cycle is equal to $\frac{m+n}{2} \times 2\pi$. Therefore, the topological charges of the corresponding beams to be equal to $\frac{m+n}{2}$.

In Fig. 4 the absolute value and phase patterns of Eq. (46) for $m = 1$ and $n = 2, 3, 4, 5$ and the corresponding beams' intensity and phase patterns are shown. As it is seen from the third column, the intensity patterns of the beams have $|m - n|$ number of asymmetric spokes. The asymmetric feature of these kinds of the beams is more dominant for $|m - n| = 1$. The intensity gradient of such beams over the transverse plane provides a lateral force on the small particles, including absorbing and dielectric micro- or nanoparticles, in the direction of intensity gradient or in the opposite direction, depending on the relative refractive index between particle and surrounding medium. To obtain a sufficient value of force to move such particles, highly focused beams can be used in practice [31,32]. By passing of a plane wave successively through one of the pure radial amplitude gratings shown in the first column and an SLM with the corresponding phase modulation given at the second column in Fig. 4, these beams can be easily generated.

VII. CATEGORIZATION OF THE SOLUTIONS

As a special form of Eq. (36), we consider $t_n = t_{-n}$, which is commonly encountered, and Eq. (36) reduces to

$$t(\theta) = t_0 + \sum_{n=1}^{+\infty} t_n \cos(n\theta), \tag{50}$$

where t_n in this equation is equal to $2t_n$ in Eq. (36). Accordingly, Eq. (37) can be rewritten as

$$U(r,\theta,z) = e^{ikz}\left\{t_0 + \sqrt{\rho}e^{i\rho}\sum_{n=1}^{+\infty} u_n \cos(n\theta) \times \left[J_{\frac{n+1}{2}}(\rho) + iJ_{\frac{n-1}{2}}(\rho)\right]\right\}, \tag{51}$$

where $u_n = \sqrt{\frac{\pi}{2}}(-i)^{\frac{n}{2}+1}t_n$. In general we call this family of results "radial carpet beams."

If we set $t_0 = 0$, the radial carpet beams take petallike forms. We call all similar cases, in which the Fourier expansion in Eq. (50) has no dc term, say $t_0 = 0$, as the dc-less transmission functions. In the following, we introduce and investigate some petallike beams of some dc-less transmission functions.

Two another special cases can be considered by eliminating t_0 and all of the terms with t_n or t_{-n} in the summation of Eq. (36),

$$t_{\pm}(\theta) = \sum_{n=1}^{+\infty} t_n \exp(\pm in\theta). \tag{52}$$

According to Eq. (37) the corresponding light beams are

$$U_{\pm}(r,\theta,z) = e^{ikz}\left\{\sqrt{\rho}e^{i\rho}\sum_{n=1}^{+\infty} u_n \exp(\pm in\theta) \times \left[J_{\frac{n+1}{2}}(\rho) + iJ_{\frac{n-1}{2}}(\rho)\right]\right\}, \tag{53}$$

where $u_n = \sqrt{\frac{\pi}{2}}(-i)^{\frac{n}{2}+1}t_n$. The main feature of this family of beams is that they carry OAM. Also the intensity profiles of these beams have ringlike shape at the lower radial distances and have twisted shape at the larger values of the radial coordinate. Therefore we call them "ringlike vortex beams." Although the name "twisted-intensity ringlike vortex beams" can be also used for such beams. Since the ringlike vortex beams carry OAM, they have potential applications in the mixing of microparticle suspensions in the optical tweezers setup.

VIII. RADIAL CARPET, PETALLIKE, AND RINGLIKE VORTEX BEAMS

In the following the recently mentioned three subfamilies of beams, the radial carpet, petallike, and ringlike vortex beams are presented by considering three radial gratings having parabolic, triangular, and modified triangular transmission profiles and by manipulating their Fourier series. The Fourier expansions of the parabolic and triangular transmission func-

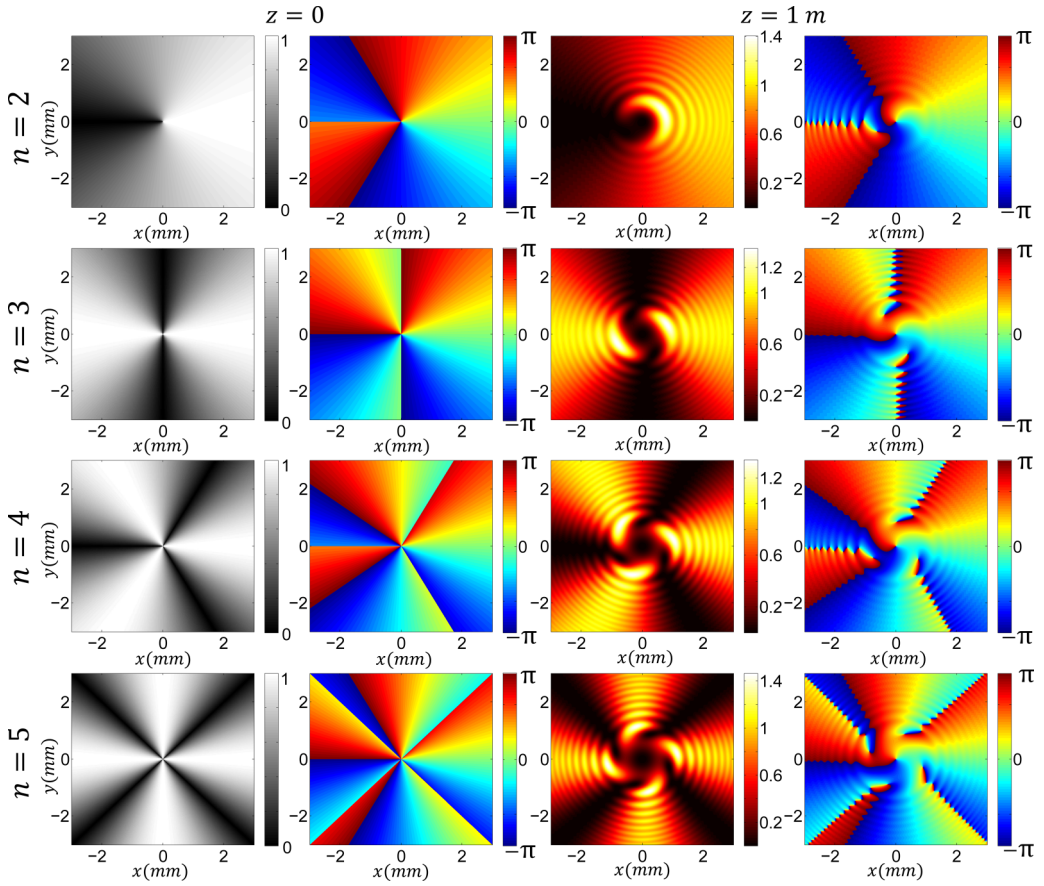

FIG. 4. First to forth rows: Absolute value (first column) and phase (second column) patterns of $t(\theta) = \frac{1}{2}(e^{im\theta} + e^{in\theta})$ and the corresponding beams' intensity (third column) and phase (forth column) patterns at $z = 1$m for $n = 2, 3, 4, 5$ and $m = 1$, respectively.

tions are given by

$$t^{\mathrm{Pa}}(\theta) = \frac{1}{3} + \sum_{q=1}^{+\infty} \frac{4}{(\pi q)^2} \cos(qm\theta) \tag{54}$$

and

$$t^{\mathrm{Tr}}(\theta) = \frac{1}{2} + \sum_{\substack{q=1 \\ \text{odd}}}^{+\infty} \frac{4}{(\pi q)^2} \cos(qm\theta), \tag{55}$$

respectively, where m is the gratings' spokes number and the "odd" under the second summation indicates that q is an odd number. The profiles of these transmission functions are illustrated in the first rows of Figs. 5 and 6 for $m = 5$, respectively. Moreover, in the first rows of Figs. 7 and 8 the absolute value and phase patterns of these transmission functions and the same patterns of the corresponding beams are shown for $m = 10$.

By eliminating the dc terms of $t^{\mathrm{Pa}}(\theta)$ and $t^{\mathrm{Tr}}(\theta)$, the following two transmission functions can be introduced:

$$t^{\mathrm{Pa}}_{t_0=0}(\theta) = \frac{3}{2} \sum_{q=1}^{+\infty} \frac{4}{(\pi q)^2} \cos(qm\theta) \tag{56}$$

and

$$t^{\mathrm{Tr}}_{t_0=0}(\theta) = 2 \sum_{\substack{q=1 \\ odd}}^{+\infty} \frac{4}{(\pi q)^2} \cos(qm\theta), \tag{57}$$

where the normalization constants $\frac{3}{2}$ and 2 are chosen so that the maximum of the absolute values of these transmittances to be 1, see the second rows of Figs. 5 and 6. The profiles of these transmission functions are illustrated in the second rows of Figs. 5 and 6 for $m = 5$. The second rows of Figs. 7 and 8 show the absolute value and phase patterns of the transmission

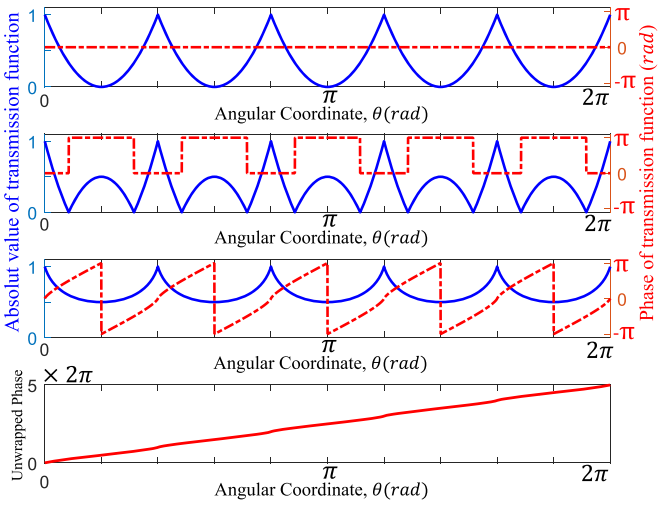

FIG. 5. First to third rows: Absolute value (blue solid line) and phase (red dash line) profiles of $t^{\mathrm{Pa}}(\theta)$, $t^{\mathrm{Pa}}_{t_0=0}(\theta)$, and t^{Pa}_{+} for $m = 5$, respectively. Forth row: Unwrapped phase profile of t^{Pa}_{+}.

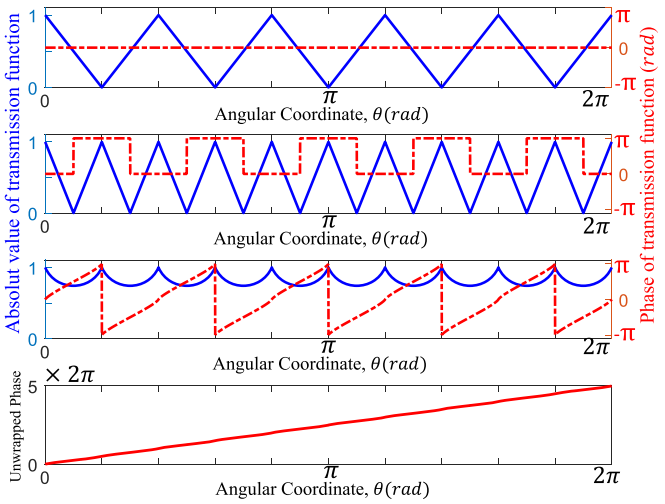

FIG. 6. First to third rows: Absolute value (blue solid line) and phase (red dash line) profiles of $t^{\mathrm{Tr}}(\theta)$, $t^{\mathrm{Tr}}_{t_0=0}(\theta)$, and t^{Tr}_{+} for $m = 5$. Forth row: Unwrapped phase profile of t^{Tr}_{+}.

functions and the same patterns of the corresponding beams for $m = 10$. As we see in these cases, the intensity profiles of the beams have a petal like shapes. It is worth noting that just by eliminating the t_0 term, the intensity profile of the resulted beams change, remarkably. It is noteworthy that the Fourier coefficients of $t^{\mathrm{Tr}}_{t_0=0}(\theta)$ have only odd indices, and as a result the period of the absolute value of the transmission function is halved in the second row of Fig. 6. The details of this effect can be found in Ref. [33].

Replacing $\cos(qm\theta)$ in Eqs. 56 and 57 by $\exp(\pm iqm\theta)$ two following transmission functions can be considered:

$$t^{\mathrm{Pa}}_{\pm}(\theta) = \frac{3}{2}\sum_{q=1}^{+\infty}\frac{4}{(\pi q)^2}\exp(\pm iqm\theta) \tag{58}$$

and

$$t^{\mathrm{Tr}}_{\pm}(\theta) = 2\sum_{\substack{q=1\\ odd}}^{+\infty}\frac{4}{(\pi q)^2}\exp(\pm iqm\theta). \tag{59}$$

The profiles of these transmission functions, with positive indices, are shown in the third rows of Figs. 5 and 6 for $m = 5$, respectively. The forth rows of these figures show the unwrapped phases of these transmission functions. We see that, in each case, the pure phase change over a cycle is equal to $m \times 2\pi$. Therefore, topological charges of the corresponding beams are equal to the spokes number m. The third rows of Figs. 7 and 8 show the absolute value and phase patterns of these transmission functions and the same patterns of the corresponding beams for $m = 10$, respectively.

As the last example and for better demonstration of the above-mentioned feathers we consider a modified form of the triangulate transmission function. The Fourier expansion of this transmission function is

$$t^{M\mathrm{Tr}}(\theta) = t_0 + \sum_{q=1}^{+\infty} t_q \cos(qm\theta), \tag{60}$$

where m is the number of spokes, $t_0 = \frac{h}{2}$, and $t_q = \frac{2}{h(q\pi)^2}[1 - \cos(q\pi h)]$, in which h is the aperture ratio or the

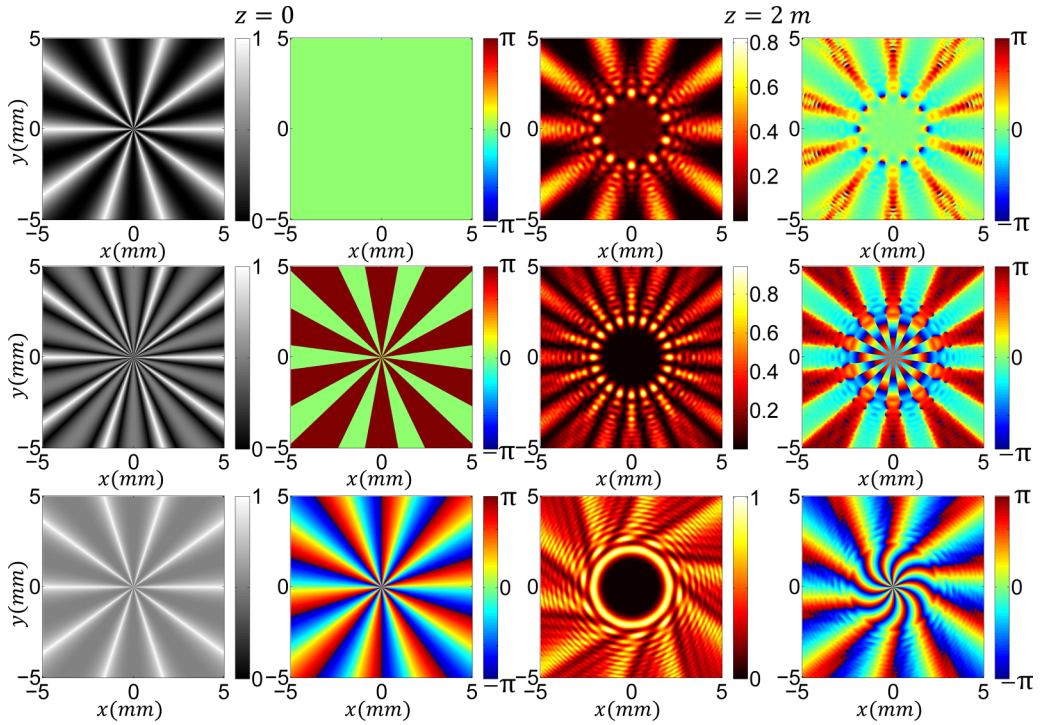

FIG. 7. Illustration of t^{Pa} (first row), $t^{\mathrm{Pa}}_{t_0=0}(\theta)$ (second row), and t^{Pa}_{+} (third row) for $m = 10$. First and second columns: Absolute value and phase patterns of the introduced transmission functions. Third and forth columns: The corresponding beams' intensity and phase patterns at $z = 2$ m. Real size of the patterns is 10 mm × 10 mm.

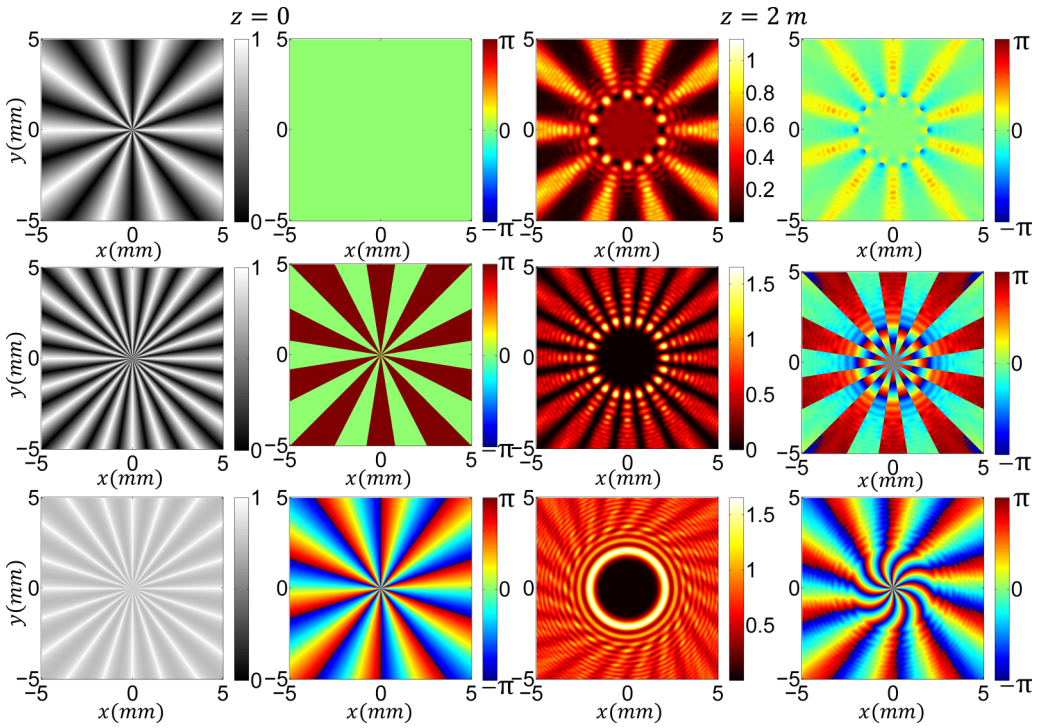

FIG. 8. The same patterns of Fig. 7 for t^{Tr}, $t^{\mathrm{Tr}}_{t_0=0}$, and t^{Tr}_{+}.

opening number of the grating. The first row of Fig. 9 shows profile of a modified triangulate transmission function with $m = 4$ and $h = 0.6$. Similar to the previous examples, the parabolic and triangular cases, here again we consider $t^{M\mathrm{Tr}}_{t_0=0}$ and $t^{M\mathrm{Tr}}_{\pm}$ transmission functions. In Fig. 9, the second and third rows show the absolute value and phase profiles $t^{M\mathrm{Tr}}_{t_0=0}$ and $t^{M\mathrm{Tr}}_{\pm}$, respectively. The forth row shows unwrapped phase profile of $t^{M\mathrm{Tr}}_{+}$ with m =4. As is apparent, a topological charge is imposed to the incident beam is equal to m. In Fig. 10, first to third columns, show the intensity (first row) and phase (second row) patterns of the beams generated by modified triangular transmission functions of $t^{M\mathrm{Tr}}$, $t^{M\mathrm{Tr}}_{t_0=0}$, and $t^{M\mathrm{Tr}}_{+}$ with $m = 15$ and $h = 0.6$, respectively.

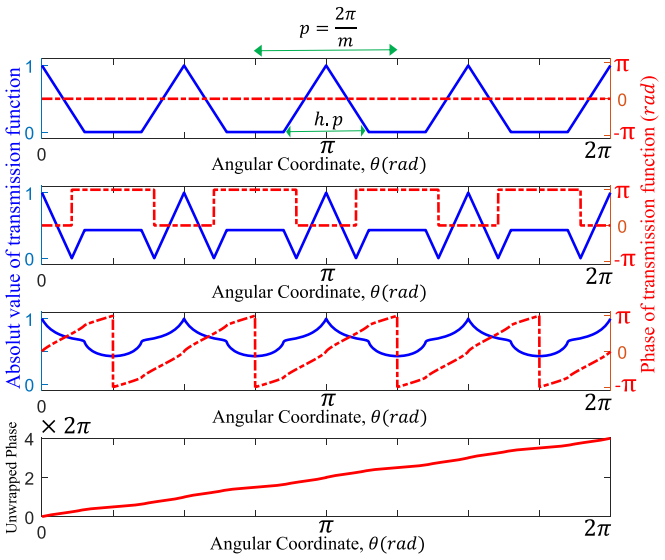

FIG. 9. First to third rows: Absolute value (blue solid line) and phase (red dash line) of $t^{M\mathrm{Tr}}(\theta)$, $t^{M\mathrm{Tr}}_{t_0=0}(\theta)$, and $t^{M\mathrm{Tr}}_{+}$ for $m = 4$ and $h = 0.6$, respectively. Fourth row: Unwrapped phase profile of $t^{M\mathrm{Tr}}_{+}$.

A close study on the diffraction of plane wave from one dimensional amplitude gratings with parabolic, triangular, and two- and three-level rectangular wave functions was presented in Ref. [33].

IX. CONCLUSION

In summary, this work presents a family of solutions of the paraxial Helmholtz equation in the cylindrical coordinates. Each of the solutions is determined by a linear combination of the Bessel functions of half-integer order. These solutions introduce a family of nondiffracting, accelerating, and self-healing beams that may carry OAM. We called them "Combined half-integer Bessel-like beams." It is shown that these beams can be generated by the diffraction of a plane wave from radial structures, so that each of this family of beams can be produced by a suitable radial structure. We showed that for a desired beam the coefficients of the corresponding linear combination of the Bessel functions are equal to the Fourier coefficients of the corresponding radial structure. In this work some interesting subfamilies of these beams were investigated. When the Fourier series of a radial structure consists of a series of terms including the dc term, in the diffraction of a plane wave from it a radial carpet beam produces. If the dc term is eliminated from the Fourier series the structure under diffraction produces a petallike beam. In this case when the coefficients of the terms with the same orders and opposite signs are equal, the beam intensity pattern at the transverse plane gets the form of a 2D optical lattice with polar symmetry [23]. If the Fourier series of a radial structure

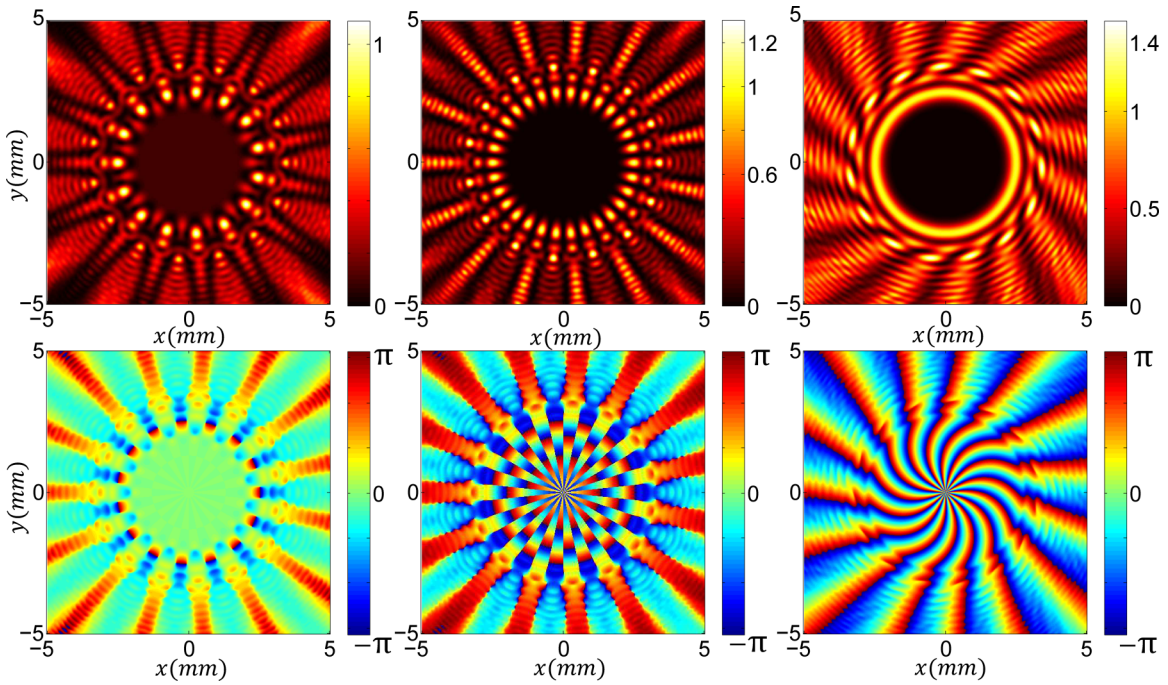

FIG. 10. First to third columns: Intensity (first row) and phase (second row) patterns of the beams generated by modified triangular transmission functions of t^{MTr}, $t^{MTr}_{t_0=0}$, and t^{MTr}_{+} at $z = 2$ m with $m = 15$ and $h = 0.6$, respectively.

consists of only the terms with the positive or negative indices, it produces ringlike beams carrying OAM that we named them ringlike vortex beams. The intensity profiles of these beams have a twisted form at the larger radial distances. Also a set of spatially asymmetric beams having half-integer OAM is introduced by special combinations of the Bessel functions of half-integer order. Since these kinds of beams have an azimuthal gradient on their intensity profiles, they can be used in changing the concentration of the microparticles in a solution. We also show that a simple vortex beam generated by an SPP belongs to the presented family of beams. As same as the radial carpet beams [23], for all the presented solutions, the self-healing feature of the beams can be verified experimentally or theoretically. A common simple approach for generating introduced beams is proposed and some applications for each of subfamilies of the introduced beams are proposed. Real generation of such beams and illustrating their applications are beyond the scope of the current work. This family of solutions of the wave equation can be found in many linear wave systems in nature, ranging from sound and elastic waves to many other kinds of classical waves.

ACKNOWLEDGMENT

This work was supported in part by the IASBS Research Council under Grant No. G2018IASBS12632.

[1] A. E. Siegman, *Lasers*, (University Science, Mill Valley, CA, 1986), Chap. 16, pp. 644–652.
[2] A. E. Siegman, Hermite-Gaussian functions of complex argument as optical-beam eigenfunctions, J. Opt. Soc. Am. **63**, 1093 (1973).
[3] T. Takenaka, M. Yokota, and O. Fukumitsu, Propagation of light beams beyond the paraxial approximation, J. Opt. Soc. Am. A **2**, 826 (1985).
[4] S. R. Seshadri, Virtual source for a Laguerre-Gauss beam, Opt. Lett. **27**, 1872 (2002).
[5] M. A. Bandres and J. C. Gutierrez-Vega, Ince-Gaussian beams, Opt. Lett. **29**, 144 (2004).
[6] M. A. Bandres, Elegant Ince-Gaussian beams, Opt. Lett. **29**, 1724 (2004).
[7] E. G. Abramochkin and V. G. Volostnikov, Hermite-Laguerre-Gaussian beams, J. Opt. A: Pure Appl. Opt. **6**, S157 (2004).
[8] D. M. Deng and Q. Guo, Elegant Hermite-Laguerre-Gaussian beams, Opt. Lett. **33**, 1225 (2008).
[9] J. C. Gutierrez-Vega and M. A. Bandres, Helmholtz-Gauss waves, J. Opt. Soc. Am. A **22**, 289 (2005).
[10] E. Karimi, G. Zito, B. Piccirillo, L. Marrucci, and E. Santamato, Hypergeometric-Gaussian modes, Opt. Lett. **32**, 3053 (2007).
[11] M. A. Bandres and J. C. Gutierrez-Vega, Cartesian beams, Opt. Lett. **32**, 3459 (2007).
[12] M. A. Bandres and J. C. Gutierrez-Vega, Circular beams, Opt. Lett. **33**, 177 (2008).
[13] J. Durnin, Exact solutions for nondiffracting beams. I. The scalar theory, J. Opt. Soc. Am. A **4**, 651 (1987).
[14] J. Durnin, J. J. Miceli, and J. H. Eberly, Diffraction-Free Beams, Phys. Rev. Lett. **58**, 1499 (1987).
[15] M. A. Bandres, J. C. Gutierrez-Vega, and S. Chavez-Cerda, Parabolic nondiffracting optical wave fields, Opt. Lett. **29**, 44 (2004).
[16] J. C. Gutierrez-Vega, M. D. Iturbe-Castillo, and S. Chavez-Cerda, Alternative formulation for invariant

optical fields: Mathieu beams, Opt. Lett. **25**, 1493 (2000).

[17] M. V. Berry and N. L. Balazs, Nonspreading wave packets, Am. J. Phys. **47**, 264 (1979).

[18] G. A. Siviloglou and D. N. Christodoulides, Accelerating finite energy Airy beams, Opt. Lett. **32**, 979 (2007).

[19] M. A. Bandres and J. C. Gutierrez-Vega, Airy-Gauss beams and their transformation by paraxial optical systems, Opt. Express **15**, 16719 (2007).

[20] J. Lu and J. F. Greenleaf, Nondiffracting X waves—Exact solutions to free-space scalar wave equation and their finite aperture realizations, IEEE Trans. Ultrason. Ferroelectr. Freq. Control **39**, 19 (1992).

[21] D. N. Christodoulides, N. K. Efremidis, P. Di Trapani, and B. A. Malomed, Bessel X waves in two- and three-dimensional bidispersive optical systems, Opt. Lett. **29**, 1446 (2004).

[22] O. Manela, M. Segev, and D. N. Christodoulides, Nondiffracting beams in periodic media, Opt. Lett. **30**, 2611 (2005).

[23] S. Rasouli, A. M. Khazaei, D. Hebri, Radial carpet beams: A class of nondiffracting, accelerating, and self-healing beams, Phys. Rev. A **97**, 033844 (2018).

[24] S. Rasouli, A. M. Khazaei, and D. Hebri, Talbot carpet at the transverse plane produced in the diffraction of plane wave from amplitude radial gratings, J. Opt. Soc. Am. A **35**, 55 (2018).

[25] D. Hebri, S. Rasouli, and M. Yeganeh, Intensity-based measuring of the topological charge alteration by the diffraction of vortex beams from amplitude sinusoidal radial gratings, J. Opt. Soc. Am. B **35**, 724 (2018).

[26] B. E. A. Saleh, M. C. Teich, and B. E. Saleh, *Fundamentals of Photonics*, Wiley Series in Pure and Applied Optics (Wiley, New York, 1991).

[27] G. B. Arfken, *Mathematical Methods for Physicists*, 3rd ed. (Academic Press, New York, 1985).

[28] A. Jeffrey and D. Zwillinger, eds. Table of integrals, series, and products (Academic Press, New York, 2007).

[29] V. V. Kotlyar, A. A. Almazov, S. N. Khonina, V. A. Soifer, H. Elfstrom, and J. Turunen, Generation of phase singularity through diffracting a plane or Gaussian beam by a spiral phase plate, J. Opt. Soc. Am. A **22**, 849 (2005).

[30] S. N. Khonina, V. V. Kotlyar, V. A. Soifer, P. Paakkonen, J. Simonen, and J. Turunen, An analysis of the angular momentum of a light field in terms of angular harmonics, J. Mod. Opt. **48**, 1543 (2001).

[31] A. Ashkin, J. M. Dziedzic, J. E. Bjorkholm, and Steven Chu, Observation of a single-beam gradient force optical trap for dielectric particles, Opt. Lett. **11**, 288 (1986).

[32] H. Rubinsztein-Dunlop, T. A. Nieminen, M. E. J. Friese, and N. R. Heckenberg, "Optical trapping of absorbing particles," In *Advances in Quantum Chemistry* (Academic Press, New York, 1998), Vol. 30, pp. 469–492.

[33] S. Rasouli and D. Hebri, Contrast enhanced quarter-Talbot images, J. Opt. Soc. Am. A **34**, 2145 (2017).